Geophys. J. Int. (1995) **123**, 887–902

On the reliability of lithospheric constraints derived from models of outer-rise flexure

Steve Mueller and Roger J. Phillips

McDonnell Center for the Space Sciences and Department of Earth and Planetary Sciences, Washington University, St Louis, MO 63130, USA

Accepted 1995 June 21. Received 1995 June 13; in original form 1995 January 20

SUMMARY

We evaluate the common practice of utilizing elastic models of outer-rise flexure to constrain lithospheric parameters, such as mechanical thickness and ambient in-plane force. We numerically compute 'synthetic' flexural profiles consistent with empirically determined constraints on lithospheric rheology and representative trench-type boundary conditions, and misfit minimization is utilized to determine the analytical solution to elastic-plate flexure that most closely resembles each synthetic profile. We then determine if it is possible to use the best-fitting elastic solutions to recover the lithospheric mechanical thickness and level of in-plane force that were assumed during the numerical computation of the synthetic profiles. This methodology is analogous to the common practice of estimating lithospheric parameters by modelling bathymetric profiles with analytical descriptions of elastic-plate flexure. Our results unequivocally indicate that in-plane force cannot be reliably constrained in this manner. Such an approach does not even allow the qualitative nature of in-plane force to be distinguished (i.e. compressional versus tensional). Although, in principle, elastic-plate models may provide reliable constraints on the mechanical thickness of oceanic lithosphere, in practice uncertainties associated with bathymetric noise and the level of in-plane force may, in some instances, render such constraints unreliable.

Key words: flexural analysis, lithospheric flexure, lithospheric structure, regional stress fields.

1 INTRODUCTION

A characteristic feature of virtually all convergent plate margins is the outer-rise complex, which is a broad gentle topographic high that is generally interpreted to represent a flexural response to the downward deflection of the subducting plate. For at least several decades, geophysicists have realized that observations of lithospheric deformation seawards of subduction zones may embody constraints on the rheology and thermal structure of oceanic lithosphere, as well as ambient levels of regional stress (i.e. in-plane force) potentially associated with the subduction process. Flexurally induced variations in seafloor topography, whether a consequence of imminent subduction or seamount loading, offer a basis from which a variety of lithospheric parameters can be deduced. The goals of lithospheric flexural modelling have been numerous; they include the following.

(1) Estimates of the limiting depth and/or temperature at which oceanic lithosphere possesses long-term strength (Caldwell & Turcotte 1979; McNutt & Menard 1982; McAdoo, Martin & Poulouse 1985).

(2) An evaluation of the validity of extrapolating laboratory measurements of rock deformation to geologically relevant strain rates (McAdoo, Caldwell & Turcotte 1978; Goetze & Evans 1979; McNutt & Menard 1982).

(3) Determination of correlations between the loading age and flexural response of oceanic lithosphere, which can provide constraints on thermal evolution. These can be used, for example, to assess whether the semi-infinite half-space thermal model or the cooling-plate thermal model represents the most accurate description of lithospheric evolution (Watts 1978; Caldwell & Turcotte 1979; Watts, Bodine & Steckler 1980).

(4) Detection of lithospheric thermal anomalies associated with intraplate volcanism (McNutt 1984).

(5) Quantification of the level of in-plane force (i.e. regional stress) associated with the process of subduction (Hanks 1971; Watts & Talwani 1974; Caldwell *et al.* 1976; McAdoo *et al.* 1978; Bodine & Watts 1979; Bodine, Steckler & Watts 1981; McAdoo & Martin 1984). Such constraints provide insight into both the nature of forces responsible for plate motions and the state of stress associated with trench-related seismicity. It has been proposed that trench congestion may result in levels of compressional in-plane force sufficient for the

nucleation of a new subduction zone within the subducting plate (Mueller & Philips 1991).

(6) Constraints on thermal gradients within the Venusian lithosphere based on observations of postulated plate flexure (Janle, Jannsen & Basilevsky 1988; Solomon & Head 1990; Sandwell & Schubert 1992; Johnson & Sandwell 1994).

The results of geophysical flexural analyses are often strikingly inconsistent. For example: (1) McNutt & Menard (1982) concluded that laboratory parametrizations of thermally activated plastic creep in olivine cannot be reliably extrapolated to geologically relevant strain rates, and that mature oceanic lithosphere has no significant long-term strength below 40 km depth. In contrast, Goetze & Evans (1979) concluded that oceanic plates obeying the relevant constitutive laboratory extrapolations support the bending moments inferred from bathymetric profiles seawards of subduction zones, and McAdoo *et al.* (1985), examining many of the same trenches as McNutt & Menard, concluded that mature oceanic lithosphere possesses significant strength to depths in excess of 60 km. (2) Flexurally based estimates of the ambient level of in-plane force seawards of the Kuril Trench have ranged from 2×10^{13} N m^{-1} compression (Hanks 1971; McAdoo *et al.* 1978), through zero (Caldwell *et al.* 1976), to 1×10^{13} N m^{-1} tension (McNutt & Menard 1982). (For purposes of comparison, a typical ridge-push force is approximately 3×10^{12} N m^{-1} compression.) (3) Sandwell & Schubert (1992) concluded that, although flexural analyses of Venusian altimetry profiles across Freyja Montes and Eithinoha Corona are consistent with thermal gradients as high as 26 and 24 K km^{-1}, respectively, flexural methods predict that the thermal gradient in other regions may be as low as 3.2 K km^{-1}. If correct, these results indicate significant regional and/or temporal variations in heat loss from the Venusian surface. The possibility that flexural analysis simply does not produce reliable constraints on lithospheric structure, however, cannot presently be ruled out.

Parsons & Molnar (1976) demonstrated that elastic-plate solutions exhibit a trade-off between end moment and in-plane force, which may account for discrepancies involving the latter, and Wessel (1992) suggested that simple visual fits are inherently unreliable. Discrepancies may also result from uncertainties associated with bathymetric or altimetric noise (i.e. topographic features not related to plate flexure; see McQueen & Lambeck 1989). We examine the additional possibility that simplifications frequently incorporated into geophysical flexural modelling are a significant factor. Specifically, many analyses of lithospheric deformation utilize elastic models of plate flexure because solutions may be conveniently determined using simple analytical methods. We perform a straightforward test of this approach to lithospheric flexural analysis. Flexural profiles consistent with both inelastic lithospheric rheology and representative trench-type boundary conditions are numerically generated and subsequently treated as 'data'. We then determine the analytical solutions to elastic models of plate flexure that exhibit the best fit to a given numerically generated 'synthetic' profile. On the basis of the best-fitting analytical solutions, we determine if it is possible to retrieve the lithospheric mechanical thickness and/or level of in-plane force assumed during the numerical computation of the synthetic profiles.

This paper is organized in the following manner. Following a brief review of geophysical flexural modelling, the differential equation governing plate flexure is introduced, and a discussion of the inelastic properties of lithosphere, emphasizing the nonlinear aspects of the moment–curvature relationship, is presented. Subsequent to a description of the manner in which the inelastic synthetic profiles are computed, the method of determining the best-fitting elastic-plate solutions is presented. Finally, efforts to recover the original 'lithospheric' parameters from the best-fitting elastic solutions are discussed.

2 METHODS OF GEOPHYSICAL FLEXURAL ANALYSIS

The simplest quantitative descriptions of sea-floor deformation are analytical models that represent the flexure of thin elastic plates (e.g. Turcotte & Schubert 1982). The lithosphere, however, does not behave in a strictly elastic manner. The uppermost lithosphere is susceptible to brittle failure, and the lowermost lithosphere is susceptible to thermally activated intracrystalline plastic creep. In these regions, yielding occurs, and the plate is unable to maintain the stress levels predicted by elastic models of plate flexure. This behaviour introduces two complications that cannot be accommodated using elastic-plate models: (1) a non-linearity in the relationship between bending moment and plate curvature; and (2) the relationship between stress and strain becomes dependent upon the deformation history of the plate.

Although modern numerical techniques permit the incorporation of inelastic rheologies into lithospheric flexural modelling, the necessary procedures are tedious. Many investigators therefore continue to utilize the simpler analytical models of elastic-plate flexure, which offer the advantage that the comparison of theoretical flexural profiles with observed bathymetry is greatly facilitated. The relationship between the elastic-model input parameters and the thermomechanical structure of the lithosphere, however, is not straightforward. For example, values of elastic-plate thicknesses derived from elastic models of lithospheric flexure are significantly less than the seismically defined thickness of the oceanic lithosphere (i.e. depth to the asthenosphere: Watts *et al.* 1980; Kirby 1983). Moreover, a direct relationship does not exist between any simple definition of oceanic lithosphere and elastic-plate thicknesses obtained in this manner. Relatively elaborate methodologies are necessary to characterize the relationship between the inferred elastic-plate thickness and the mechanical structure of the lithosphere (e.g. McNutt & Menard 1982; McNutt 1984). In contrast, inelastic flexural models, which incorporate realistic lithospheric rheologies, possess the advantage that model input parameters associated with the thermomechanical structure of the lithosphere directly correspond to lithospheric parameters.

Essentially, there are two approaches to geophysical flexural analysis. The first alternative (hereafter referred to as Method I) utilizes analytical descriptions of elastic-plate flexure to model observations. In this case, the modelling stage is greatly simplified, but the relationship between the modelling results and lithospheric parameters may be unclear. The second alternative (hereafter referred to as Method II) utilizes inelastic models of plate flexure, requiring numerically elaborate efforts but offering a straightforward interpretation of results. Representative examples of Method I flexural analysis include Caldwell *et al.* (1976), Caldwell & Turcotte (1979), McNutt & Menard (1982), McNutt (1984), Judge & McNutt (1988), Solomon & Head (1990), and Sandwell & Schubert (1992).

Representative examples of Method II flexural analysis include McAdoo *et al.* (1978, 1985), Turcotte, McAdoo & Caldwell (1978), Bodine & Watts (1979), and Bodine *et al.* (1981).

Method I flexural analyses embody the implicit assumption that, for a specified lithospheric thermomechanical structure, a hypothetical elastic plate exists that will closely mimic the flexural response of the inelastic lithosphere. A number of early studies pursued the possibility that the thickness of this elastic plate, T_e, corresponded to the depth of a particular mantle isotherm (e.g. Watts 1978; Caldwell & Turcotte 1979). McNutt & Menard (1982) have presented a convincing argument, however, that any correspondence between T_e and lithospheric mechanical structure cannot be independent of plate curvature. Larger values of plate curvature induce greater degrees of bending-induced failure, which decreases the portion of the lithosphere that behaves elastically, and T_e is reduced accordingly. For this reason, T_e, the 'effective elastic thickness' of the lithosphere, is likely to be dependent upon plate curvature and must always be less than T_m, the 'effective mechanical thickness' of the lithosphere (the latter is defined as the greatest depth at which the lithosphere possesses any significant long-term strength) (McNutt & Menard 1982). McNutt & Menard (1982) proposed a relationship between T_e and T_m that is based on the requirement that the purely elastic plate and the lithospheric plate support identical bending moments at a specified curvature.

There are two methods commonly employed to estimate T_e from bathymetric profiles seawards of subduction zones. The simplest (e.g. Caldwell *et al.* 1976; Caldwell & Turcotte 1979; McNutt & Menard 1982) invokes a relationship between T_e and the distance between the outer-rise crest and the 'first zero-crossing' (the latter is defined as the point between the trench axis and the outer-rise crest where the subducting seafloor crosses the depth of the abyssal plain seawards of the outer rise). Using the parameters in Table 1, this relationship is (e.g. Caldwell & Turcotte 1979) $T_e + (0.01369\ \mathrm{m}^{-1/3})(x_b - x_{zc})^{4/3}$, where x_b indicates the location of the outer-rise crest and x_{zc} indicates the location of the first zero-crossing. Estimates of T_e obtained in this manner are representative only of oceanic lithosphere located seawards of the first zero-crossing. Although the region seawards of x_{zc} is typically characterized by small plate curvatures and minimal amounts of flexurally induced yielding (which, in theory, permits a closer correspondence between T_e and T_m), it is also a region of gentle variations in flexurally induced topography, where bathymetric noise can seriously frustrate efforts to constrain both x_b and x_{zc} (e.g. Caldwell *et al.* 1976; McAdoo *et al.* 1978).

Estimates of T_e are also derived by varying the input parameters of analytical models of elastic-plate flexure until minimal misfit with respect to the observed bathymetry is obtained. This is typically accomplished with simple visual comparisons, although least-squares methods are occasionally employed (e.g. Solomon & Head 1990; Sandwell & Schubert 1992; Johnson & Sandwell 1994). This approach requires a greater effort than the previous alternative, yet possesses the advantage that estimates of T_e are influenced by the entire bathymetric profile, and the results are therefore relatively insensitive to the exact location of any particular point. For example, critically located volcanic constructs may preclude estimates of T_e based on the locations of x_b and x_{zc}, whereas misfit minimization might still produce useful results in these circumstances.

Table 1. Parameter values referred to in the text. When different, Venusian values are indicated parenthetically.

Parameter	Value
Gravitational acceleration g	9.8 (8.87) m/sec^2
Density contrast across plate $\Delta\rho$	2300 (3300) kg/m^3
Young's modulus E	65 GPa
Poisson's ratio ν	0.25
Asthenospheric temperature	1650 K
Surface temperature	270 (740) K
Thermal plate thickness	125 km
Thermal diffusivity	1.2 x 10^{-6} m^2/sec
Universal gas constant R	8.314 J/mol-K
$\dot{\varepsilon}_{0l}$	7.0 x 10^{14} sec^{-1}
$\dot{\varepsilon}_{0h}$	5.7 x 10^{11} sec^{-1}
σ_p	8.5 x 10^9 Pa
Q_l	5.23 x 10^5 J/mol
Q_h	5.49 x 10^5 J/mol
n	3

3 VON KÁRMÁN EQUATION FOR PLATE FLEXURE

Elastic–plastic flexural profiles [i.e. synthetic bathymetry (Earth) and altimetry (Venus)] are computed using the von Kármán equation of plate deflection (Fung 1965). We define the vertical dimension, z, as depth (i.e. positive downwards). The top and bottom plate boundaries are located at $z = 0$ and $z = +T_m$, respectively. Because the von Kármán equation represents a force–torque balance, it is not necessary at this stage to specify rheology. We adopt a sign convention in which tensional normal stresses are positive, and positive plate curvature is concave downwards. Defining x as the horizontal dimension, the complete von Karman equation is (Fung 1965)

$$\frac{\partial^2 M(x)}{\partial x^2} = -\frac{\partial N(x)}{\partial x}\frac{\partial w(x)}{\partial x} - N(x)\frac{\partial^2 w(x)}{\partial x^2} - \sigma_{zz}(x, T_m) + \sigma_{zz}(x, 0) - \int_0^{T_m} Z(x)\,dz - \int_0^{T_m}\left(z - \frac{T_m}{2}\right)\frac{\partial X(x)}{\partial x}\,dz - \frac{T_m}{2}\left[\frac{\partial \sigma_{zx}(x, T_m)}{\partial x} + \frac{\partial \sigma_{zx}(x, 0)}{\partial x}\right] - \sigma_{zx}(x, T_m)\frac{\partial w(x)}{\partial x} + \sigma_{zx}(x, 0)\frac{\partial w(x)}{\partial x}, \quad (1)$$

where $w(x)$ is vertical displacement; $Z(x)$ and $X(x)$ are body forces in the z- and x-directions, respectively; $\sigma_{zz}(x, 0)$ and $\sigma_{zz}(x, T_m)$ are vertical normal stresses externally applied to the top and bottom of the plate, respectively; and $\sigma_{zx}(x, 0)$ and $\sigma_{zx}(x, T_m)$ are shear tractions externally applied to the top and bottom of the plate, respectively. $N(x)$ represents the in-plane force (units of N m^{-1}), often referred to as the 'regional stress':

$$N(x) = \int_0^{T_m} \sigma_{xx}(x, z)\,dz, \quad (2)$$

and $M(x)$ represents the bending moment (units of N):

$$M(x) = \int_0^{T_m}\left(z - \frac{T_m}{2}\right)\sigma_{xx}(x, z)\,dz, \quad (3)$$

in which $\sigma_{xx}(x, z)$ is the horizontal normal stress. Because the

bending moment is defined about the mid-point of the plate in the derivation of the von Kármán equation (Fung 1965), mathematical consistency requires that it also be defined about the mid-point of the plate in eq. (3).

Several terms included in the von Kármán equation are not relevant to subducting oceanic lithosphere. Because we are modelling regions seawards of the trench axis, there is no shear force applied to the top of the plate, and $\sigma_{zx}(x, 0)$ is zero. On Earth, the low-viscosity asthenosphere effectively decouples stress associated with mantle convection from stress that exists within the oceanic lithosphere (e.g. Forsyth & Uyeda 1975; Chapple & Tullis 1977; Melosh 1977; Wiens & Stein 1985; Craig & McKenzie 1986), and this precludes any significant level of shear traction from being exerted on the lower plate surface. Accordingly, $\sigma_{zx}(x, T_m)$ is also assumed to be zero. [Note, however, that this may not be the case for Venus (e.g. Phillips 1990).] We further assume that local gravitational body forces in the z-direction are negligible in contrast to vertical loading [i.e. $\sigma_{zz}(x, 0)$, $\sigma_{zz}(x, T_m)$, and boundary conditions at the trench]. The vertical normal stress applied to the bottom of the plate, $\sigma_{zz}(x, T_m)$, represents the restoring force (sometimes referred to as the Winkler force) induced in response to displacement of the underlying material. Thus

$$\sigma_{zz}(x, T_m) = -\Delta\rho g w(x), \tag{4}$$

where $\Delta\rho$ is the density difference between material that exists below and above the plate (Table 1), and g is the relevant gravitational acceleration. The minus sign indicates that this stress always opposes displacement. Vertical normal stress applied to the upper plate surface, $\sigma_{zz}(x, 0)$, is associated with sediment accumulation, seamount loading, etc. These assumptions, combined with the additional assumption of constant in-plane force (justified below), eliminate several of the terms included in eq. (1), leaving

$$\frac{d^2M(x)}{dx^2} = -N(x)\frac{d^2w(x)}{dx^2} + \Delta\rho g w(x) + \sigma_{zz}(x, 0). \tag{5}$$

The rheology-dependent relationship between bending moment, $M(x)$, and plate curvature, $d^2w(x)/dx^2$, must be established before solutions to eq. (5) can be determined. Elastic plates possess a linear moment–curvature relationship, and analytical solutions to eq. (5) often exist. Inelastic (i.e. elastic–plastic) plates possess a non-linear moment–curvature relationship, and solutions to eq. (5) must be determined numerically (non-uniqueness may also be a problem). The manner in which the moment–curvature relationship is determined for various lithospheric rheologies is described in the following section.

With the substitutions $Y_1(x) = dM(x)/dx$, $Y_2(x) = M(x)$, $Y_3(x) = w(x)$, and $Y_4(x) = dw(x)/dx$, eq. (5) can be reduced to a system of four first-order differential equations (e.g. Phillips 1990):

$$\frac{dY_1(x)}{dx} = -N(x)[f^{-1}\{Y_2(x)\}] + \Delta\rho g Y_3(x) + \sigma_{zz}(x, 0), \tag{6}$$

$$\frac{dY_2(x)}{dx} = Y_1(x), \tag{7}$$

$$\frac{dY_3(x)}{dx} = Y_4(x), \tag{8}$$

$$\frac{dY_4(x)}{dx} = f^{-1}\{Y_2(x)\}, \tag{9}$$

where $M(x) = Y_2(x) = f\{d^2w(x)/dx^2\}$ represents the non-linear moment–curvature relationship. $d^2w(x)/dx^2$ $(= dY_4(x)/dx)$ is obtained by inverting the functional relationship between bending moment and plate curvature, or, in other words, $d^2w(x)/dx^2 = f^{-1}\{Y_2(x)\}$. Bending moments are determined for a regular distribution of plate curvatures, and an interpolative splining routine is utilized to provide a continuous moment–curvature relationship. A variety of numerical techniques can be used to solve eqs (6)–(9), which constitute a two-point boundary-value problem.

4 EFFECTS OF LITHOSPHERIC INELASTICITY

4.1 Yield envelopes and the moment–curvature relationship

For an elastic plate, the bending moment (M) is proportional to curvature ($dw^2(x)/dx^2$), and analytical solutions to eq. (5) generally exist. Analytical models of elastic-plate flexure are adequate provided that the lithosphere is subjected to relatively small degrees of failure. Numerical models of inelastic-plate flexure are necessary, however, when bending and/or in-plane force induce non-negligible amounts of failure. In this case, the moment–curvature relationship is non-linear, and solutions to eq. (5) must be determined numerically.

Depth-dependent lithospheric yield strength is governed by brittle failure (i.e. faulting) in the upper, cold lithosphere, and plastic failure in the lower, hot lithosphere. We assume that brittle yield strength is governed by slip along pre-existing faults, rather than the rupture strength of intact rock (e.g. Goetze & Evans 1979; Brace & Kohlstedt 1980; Bodine *et al.* 1981; McNutt & Menard 1982). Byerlee (1978) determined that the frictional resistance to fault slip is essentially independent of temperature, strain rate, and (with a few exceptions that are not relevant to our analysis) rock composition. Using relationships derived in Jaeger & Cook (1976; based on the results of Byerlee), which optimize the likelihood of brittle failure by permitting slip to occur along the theoretically least-resistive fault orientation, the following expressions are obtained for brittle lithospheric strength ($\Delta\sigma$) in tension:

$$\Delta\sigma = \begin{cases} (0.786)\bar{\sigma}_v & \bar{\sigma}_v \le 529.9 \text{ MPa}, \\ 56.7 \text{ MPa} + (0.679)\bar{\sigma}_v & \bar{\sigma}_v \ge 529.9 \text{ MPa}, \end{cases} \tag{10}$$

and compression:

$$\Delta\sigma = \begin{cases} -(3.68)\bar{\sigma}_v & \bar{\sigma}_v \ge 113.2 \text{ MPa}, \\ -176.6 \text{ MPa} - (2.12)\bar{\sigma}_v & \bar{\sigma}_v \le 113.2 \text{ MPa}. \end{cases} \tag{11}$$

$\bar{\sigma}_v$ is the effective vertical stress (i.e. lithostatic overburden minus ambient water pore pressure). The derivations of eqs (10) and (11) are included in the Appendix. We assume that hydrostatic pore pressures exist within the igneous portion of the oceanic lithosphere. Sea-floor drill holes that fully penetrate the sedimentary veneer rarely induce a vertical flow of water, which would be expected if non-hydrostatic pore pressures were encountered (e.g. Hyndman, Langseth & von Herzen 1987). Pore pressures are assumed to be zero for calculations relevant to Venusian lithosphere.

In the lower lithosphere, yield strength is limited by thermally activated intracrystalline plastic creep, a process that we quantify using the following relationship between temperature

(T), strain rate ($\dot{\varepsilon}$), and yield strength ($\Delta\sigma$) in olivine (Goetze & Evans 1979):

$$\Delta\sigma = \begin{cases} [(\dot{\varepsilon}/\dot{\varepsilon}_{0l})\exp(Q_l/RT)]^{1/n} & \Delta\sigma < 200\ \text{MPa}, \\ \sigma_p[1 - \sqrt{(RT/Q_h)\ln(\dot{\varepsilon}_{0h}/\dot{\varepsilon})}] & \Delta\sigma > 200\ \text{MPa}, \end{cases} \quad (12)$$

the subscripts l and h stand for low and high, respectively. The constants in this expression are defined in Table 1 [note that, whereas Q_l is adopted directly from Goetze & Evans (1979), Q_h is calculated to enforce continuity at 200 MPa]. Because plastic failure is a non-dilatational process, lithospheric strength within the plastic regime is the same in compression and tension. Our models consistently predict that the yield strength of the oceanic lithosphere is governed by brittle failure to a depth of at least ten kilometres, and it is therefore unnecessary to include a separate plastic flow law for the basaltic crust (although this is not necessarily the case for Venus).

A strain rate of $10^{-16}\,s^{-1}$ is assumed to represent plastic failure (i.e. geophysically significant creep), consistent with McNutt & Menard (1982), McNutt (1984), McAdoo *et al.* (1985), Solomon & Head (1990) and Sandwell & Schubert (1992). Temperature, as a function of depth and plate age, is modelled using the cooling-plate model (Parsons & Sclater 1977), using the parameter values in Table 1. Because the primary heat-loss mechanism of Venus has not been unequivocally identified (e.g. Kaula & Phillips 1981; Solomon & Head 1982; Morgan & Phillips 1983; Phillips & Malin 1983), we simply assume a range of linear thermal gradients and a surface temperature of 740 K. If the 'bottom' of the plate is defined as the depth, T_m, at which the plastic shear resistance equals 50 MPa (e.g. McNutt & Menard 1982; McNutt 1984), eqs (10)–(12) describe a lithospheric 'yield envelope'. Representative examples of oceanic and Venusian lithospheric yield envelopes are illustrated in Fig. 1. Because the stress level at a particular depth cannot exceed the associated yield strength, lithospheric stress profiles remain bounded by the relevant yield envelope. Attempts to increase the applied stress beyond the yield-strength value result in further deformation and do not induce a compensating increase of stress within the lithosphere. If the applied stress equals the yield strength, essentially limitless deformation is possible, provided that the applied stress is maintained at this level.

As a segment of oceanic lithosphere (subjected to zero in-plane force) migrates into a subduction zone, it begins to experience shallow, brittle, extensional failure, and deep, plastic, compressional failure, both in response to plate bending within the outer-rise complex. Because brittle failure is potentially seismogenic, the shallow extensional failure is generally regarded as the source of shallow, normal-faulting, outer-rise earthquakes. (The deeper, complementary compressional failure is presumably aseismic because it is accommodated by plastic deformation.) When the degree of plate bending is moderate, these two regions of failure are separated by an elastic 'core', in which bending stresses do not exceed local yield-strength values.

The tectonic stress profile (defined as total stress minus lithostatic stress) associated with zero in-plane force, a plate age of 100 Ma, and lithospheric bending to a plate curvature, C, of $+3 \times 10^{-7}\,m^{-1}$ (positive plate curvature is representative of outer-rise flexure) is shown in Fig. 2(a). Stresses within the

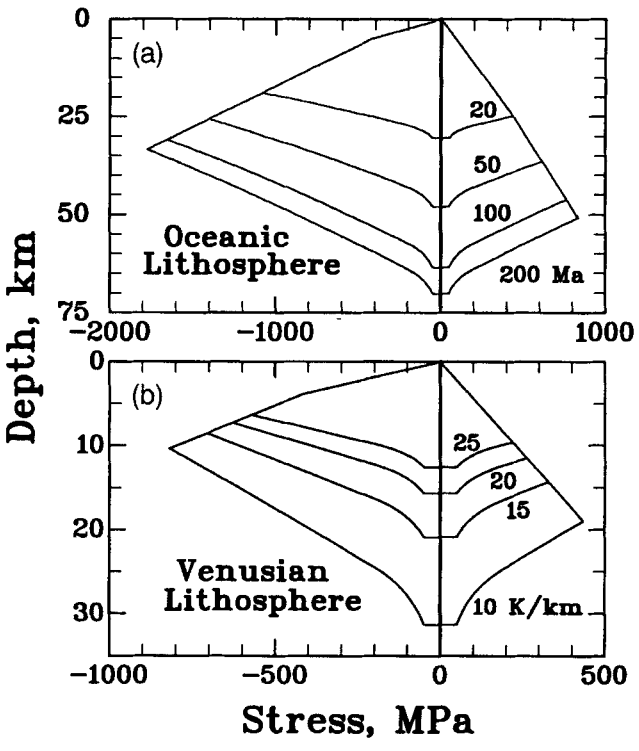

Figure 1. Representative lithospheric yield envelopes. Yield strength is governed by brittle failure within the upper cold lithosphere and intracrystalline plastic creep within the lower hot lithosphere. Tensional normal stress is positive and a strain rate of $1 \times 10^{-16}\,s^{-1}$ is assumed to represent plastic failure. The net tensional lithospheric strength is determined by integrating the $\Delta\sigma > 0$ portion of the yield envelope, and the net compressional strength by an integration of the $\Delta\sigma < 0$ portion. (a) Oceanic lithosphere. Hydrostatic pore pressure and a cooling-plate thermal model are assumed. (b) Venusian lithosphere. Zero pore pressure and constant thermal gradients are assumed.

elastic core are related to the plate curvature, $d^2w(x)/dx^2$, by

$$\Delta\sigma(z) = \frac{-E(z - z_0)}{(1 - \nu^2)} \frac{d^2w(x)}{dx^2}, \quad (13)$$

where E is Young's modulus and ν is Poisson's ratio (Table 1). The term z_0, which represents the depth at which the stress within the elastic core equals zero, is specified by the condition that the stress profile should integrate to the assumed value of in-plane force. The bending moment associated with this stress distribution is determined by eq. (3). As the plate curvature approaches extreme values (e.g. the broken line in Fig. 2a), the elastic core thickness approaches zero, and the bending moment begins to 'saturate'. At this point, an additional increase in the plate curvature does not induce a significant increase in the bending moment that is supported within the plate, and a 'plastic hinge' develops. Conversely, if the applied bending moment reaches the saturation value, the plate curvature may be increased indefinitely with no additional increase in the applied moment (thus the analogy to a hinge). Oceanic lithosphere possesses two characteristic saturation bending moments: one associated with positive plate curvature, and one associated with negative plate curvature. Because of the asymmetry of the lithospheric yield envelope, the two saturation moments are generally unequal.

The moment–curvature relationship for 100 Ma oceanic

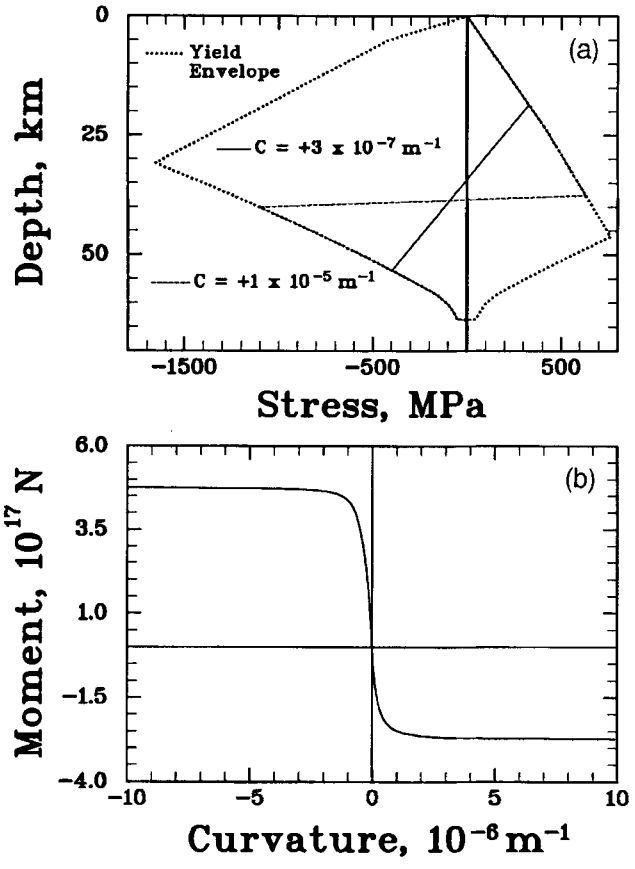

Figure 2. Representative flexurally induced tectonic stress profiles and moment–curvature relationship for 100 Ma oceanic lithosphere subjected to zero in-plane force. (a) Stress profiles for plate curvature of $+3 \times 10^{-7}\,\mathrm{m}^{-1}$ (solid line) and $+1 \times 10^{-5}\,\mathrm{m}^{-1}$ (broken line). (b) Moment–curvature relationship. At excessive curvatures, moment saturation occurs and additional increases in curvature are possible without an increase in the applied bending moment.

lithosphere subjected to zero in-plane force is shown in Fig. 2(b). Small plate curvatures, which result in minimal yielding, are associated with a moment–curvature relationship that is essentially elastic (i.e. linear). The rate of change of bending moment with respect to small degrees of plate curvature is

$$\frac{dM}{dC} = \frac{-ET_m^3}{12(1-\nu^2)}, \tag{14}$$

where T_m is the lithospheric mechanical thickness. In this case, dM/dC is simply the flexural rigidity defined in elastic-plate theory. Extreme values of bending moment (or, equivalently, plate curvature) are associated with a non-unique moment–curvature relationship, and solutions to eqs (6)–(9) are also non-unique.

4.2 Stress history and the moment–curvature relationship

Stress reduction within a region of active failure induces 'elastic unloading'. (In the present context, stress 'reduction' refers merely to a decrease in the absolute value of the applied stress.) Regardless of the amount of deformation sustained during failure, if the stress level drops below the critical yield-strength value, the material will respond elastically. Elastic unloading occurs along a different stress–strain path from the original loading process. The relationship between stress and strain is initially linear because the applied stress is less than the yield value. If the applied stress achieves, and is maintained at, the yield value, unlimited strain becomes possible. When the applied stress drops below this value the material responds elastically and a linear relationship, once again, exists between stress and strain. Although the stress returns to zero, the strain retains a 'memory' of failure in the form of permanent deformation (i.e. strain hysteresis).

An example is represented by the 'unbending' of oceanic lithosphere. The maximum plate curvature within the outer-rise complex typically occurs midway between the trench axis and the first zero-crossing, provided that a significant bending moment does not exist at the trench axis (e.g. McAdoo *et al.* 1978; Turcotte *et al.* 1978; Bodine & Watts 1979; Bodine *et al.* 1981). Much of the outer trench wall is therefore a region of decreasing plate curvature. A decrease in the plate curvature promotes elastic unloading in previously failed portions of the plate, and a 'memory' of failure, which influences the subsequent flexural response, is introduced into the stress profile. The tectonic stress profile associated with zero in-plane force, 100 Ma sea-floor, and an initial plate curvature of $+3 \times 10^{-7}\,\mathrm{m}^{-1}$ is represented by the broken line in Fig. 3(a). If the curvature is increased, neither unbending nor elastic unloading occurs. If the curvature is decreased, however, previously failed regions at the top and bottom of the plate will respond elastically to the resulting decrease in the ambient stress level. In this case, plate unbending induces a pattern of failure opposite to the original pattern: compressional failure in the upper, brittle portion of the lithosphere, and extensional failure in the lower, plastic portion. Note that this occurs despite the fact that the plate curvature remains positive.

The solid line in Fig. 3(a) represents the stress profile associated with the unbending of a lithospheric plate to a final curvature of $+2 \times 10^{-7}\,\mathrm{m}^{-1}$ from an initial (i.e. maximum) curvature of $+3 \times 10^{-7}\,\mathrm{m}^{-1}$. The final stress distribution is derived from the initial stress distribution (broken line, Fig. 3a) by the subtraction of an elastic (i.e. linear) stress distribution (eq. 13). The gradient of the subtracted elastic stress distribution, $d(\Delta\sigma)/dz$, is determined by eq. (13) with the unbending plate curvature (in this case, $+2 \times 10^{-7}\,\mathrm{m}^{-1}$) equal to $d^2w(x)/dx^2$, and the intercept, z_0, iteratively determined by the requirement that the final stress distribution integrate to the assumed level of in-plane force. Where subtraction of the elastic stress distribution violates the yield envelope, the yield-strength value limits the local tectonic stress. Although the final stress distribution in Fig. 3(a) may seem contrary to intuition (i.e. 'zig-zags' within the elastic core), stress reversal during elastic unloading is a well-documented engineering phenomenon (e.g. Drucker 1967; Johnson & Mellor 1973).

The manner in which this behaviour affects the moment–curvature relationship is illustrated in Fig. 3(b). The broken line represents the original moment–curvature relationship, and the solid line represents the moment–curvature relationship associated with unbending from a plate curvature of $+3 \times 10^{-7}\,\mathrm{m}^{-1}$. The permanent deformation of the plate accumulated during the initial episode of prograde bending is reflected in the failure of the unbending curve to pass through the origin. The behaviour represented in Fig. 3(b) is quite intuitive. If an initially straight elastic–plastic (e.g. metal) bar

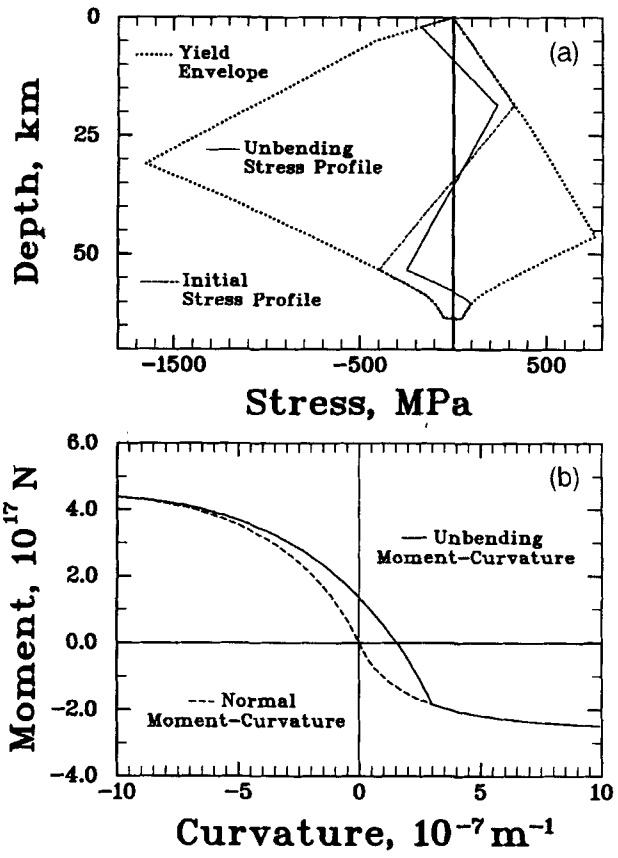

Figure 3. Representative tectonic stress profile and moment–curvature relationship associated with the unbending of 100 Ma oceanic lithosphere subjected to zero in-plane force. (a) Stress profile associated with a reduction in plate curvature from an initial value of $+3 \times 10^{-7}$ m^{-1} (broken line) to a final value of $+2 \times 10^{-7}$ m^{-1} (solid line). A reduction of the plate curvature introduces a 'memory' of failure into the stress distribution. (b) Moment–curvature relationship. The broken line is identical to the curve in Fig. 2(b). The solid line represents the moment–curvature relationship that governs plate unbending from a maximum curvature $+3 \times 10^{-7}$ m^{-1}. The permanent deformation accumulated during prograde bending is reflected in the failure of the unbending moment–curvature relationship to pass through the origin.

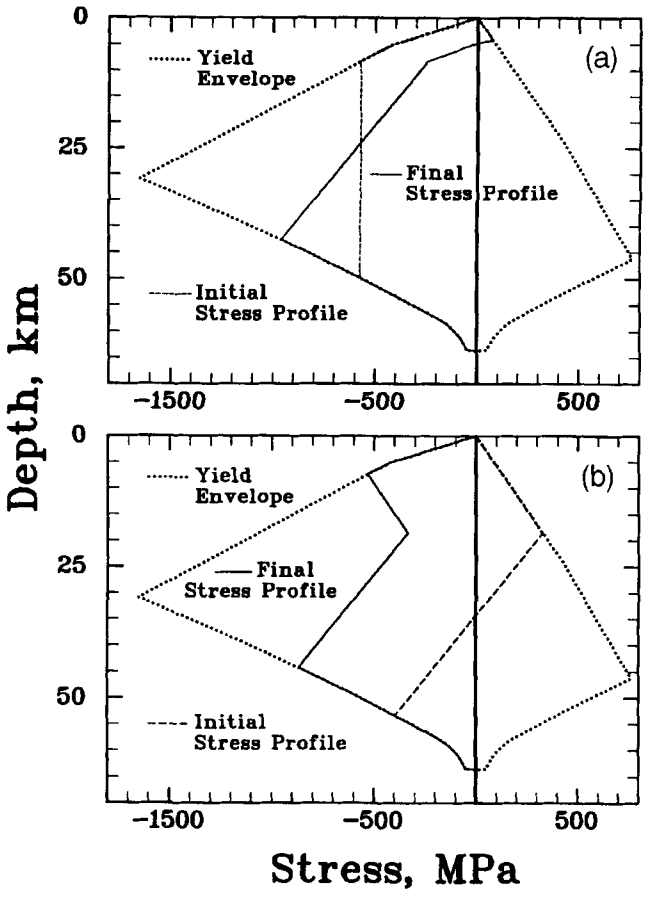

Figure 4. Tectonic stress profiles associated with a combination of plate bending and in-plane compression (100 Ma oceanic lithosphere). Broken lines represent initial stress distributions and solid lines represent final stress distributions. (a) The broken line represents the stress profile associated with zero plate curvature and a compressional in-plane force of -3×10^{13} N m^{-1}. The solid line indicates the stress profile that results from the subsequent prograde bending of the plate to a curvature of $+3 \times 10^{-1}$ m^{-1}. (b) The broken line represents the stress profile associated with zero in-plane force and prograde plate bending to a curvature of $+3 \times 10^{-7}$ m^{-1}. The solid line indicates the stress profile that results from the subsequent application of -3×10^{13} N m^{-1} of compressional in-plane force.

is flexed and released, it will not resume its original shape. Instead, it will rebound to a non-zero curvature that is less than the curvature maintained at the time of release. At this point, the bar possesses zero bending moment (because it has been released) and non-zero curvature. A bending moment opposite to that initially exerted must be applied if the bar is to be returned to a straight configuration (i.e. zero curvature). The magnitude of this bending moment depends upon the material properties of the bar.

Although several elastic–plastic flexural modelling studies have recognized the significance of elastic unloading during plate unbending (e.g. McAdoo *et al.* 1978; Turcotte *et al.* 1978; Bodine & Watts 1979; Bodine *et al.* 1981), the effects associated with in-plane force have not been addressed. If, in the absence of plate bending, 100 Ma oceanic lithosphere is subjected to a compressional in-plane force of -3×10^{13} N m^{-1}, the resulting stress profile is illustrated by the broken line in Fig. 4(a). [The value of in-plane force incorporated slightly exceeds one-half of the compressional strength of oceanic lithosphere of this age, and is potentially representative of regional stress levels associated with trench congestion (e.g. McAdoo & Sandwell 1985; Cloetingh & Wortel 1986; Zuber 1987; Mueller & Phillips 1991)]. Compressional failure occurs within the upper and lower plate extremities, a uniform value of tectonic stress exists within the elastic core (reflecting zero plate curvature), and the integral of the tectonic stress distribution equals the applied in-plane force. Now assume that a segment of oceanic lithosphere represented by such a stress distribution migrates into an outer-rise complex. The associated plate bending enhances the amount of compression at the bottom of the plate, and compressional failure therefore extends further upward into the lower portion of the lithosphere. In contrast, plate bending promotes stress reduction within the failed portion of the upper lithosphere, resulting in the elastic unloading of the zone of brittle failure. The resulting distribution of tectonic stress is illustrated by the solid line in Fig. 4(a) for a plate curvature of $+3 \times 10^{-7}$ m^{-1}. The solid line is derived from the broken line

using the procedure described above for plate unbending. In the upper extremities of the plate, elastic unloading perturbs the pre-existing stress distribution sufficiently to induce brittle extensional failure. Also, the tectonic stress profile within the elastic core exhibits a kink, which separates lithosphere possessing a 'memory' of failure (upper portion of the elastic core) from lithosphere that has behaved elastically throughout (lower portion of the elastic core). The slope $[d(\Delta\sigma)/dz]$ within this latter region is defined by eq. (13), with $d^2w(x)/dx^2$ equated with the final plate curvature.

Now consider a reversal of the above plate-loading scenario. The broken line in Fig. 4(b) represents the tectonic stress profile associated with 100 Ma oceanic lithosphere, zero in-plane force, and a plate curvature of $+3 \times 10^{-7}\ \mathrm{m}^{-1}$. The subsequent application of $-3 \times 10^{13}\ \mathrm{N\,m}^{-1}$ of compressional in-plane force induces an upward migration of the zone of compressional failure within the lower lithosphere. In contrast, elastic unloading occurs throughout the region previously subjected to bending-induced extensional brittle failure. The resulting stress profile (solid line, Fig. 4b) is derived by adding a constant stress level (in this case negative) to the initial stress profile. Once again, where violation of the yield envelope is indicated, local yield-strength limits tectonic stress. The magnitude of the added stress level is iteratively determined by the requirement that the final stress distribution integrate to the assumed value of the in-plane force. Once again, a kink within the elastic core separates lithosphere possessing a memory of failure from that which does not.

Differences between the final stress profiles in Fig. 4 illustrate that a reversal of plate-loading order (i.e. bending versus in-plane force) may have important consequences and represent a significant source of non-uniqueness in flexural solutions (i.e. the final plate configuration depends upon the loading history). For example, the bending moment associated with the final stress distribution in Fig. 4(b) is only 15 per cent of that associated with the final stress distribution in Fig. 4(a). The seismic implications of this behaviour are significant. For example, patterns of brittle failure represented in the final stress distributions of Fig. 4 illustrate that either normal-faulting or thrust-faulting outer-rise seismicity may be associated with significant levels of compressional in-plane force. The extensional brittle failure indicated by the final stress distribution in Fig. 4(a) illustrates that the occurrence of normal-faulting earthquakes seawards of the trench axis is not inconsistent with the existence of significant levels of compressional in-plane force.

If migrating oceanic lithosphere encounters significant levels of in-plane force seawards of the outer-rise complex, the most appropriate representation of the loading history is that depicted in Fig. 4(a). Alternatively, if oceanic lithosphere subducting in the absence of any significant level of in-plane force is subjected to the geologically sudden application of such a force, perhaps in response to the onset of trench congestion, the most appropriate representation of plate-loading history is that illustrated in Fig. 4(b). In reality, the level of in-plane force is likely to vary with distance from the trench axis, and the examples presented merely represent end-member simplifications that illustrate the relationship between outer-rise dynamics and plate-loading history.

5 SYNTHETIC FLEXURAL PROFILES

After determining lithospheric moment–curvature relationships that are consistent with eqs (10)–(12), we numerically determine solutions to the von Kármán equation assuming trench-type boundary conditions. The resulting flexural profiles represent synthetic bathymetry (Earth) and altimetry (Venus). Boundary conditions at the trench axis ($x = 0$) are zero bending moment and a downward displacement equal to w_0. Although there is no rigorous justification for the assumption of zero bending moment as a boundary condition, Hanks (1971) has argued that, in general, the point of zero moment should be somewhere in the vicinity of the trench axis. Moreover, the assumption of zero end moment is implicit in all 'broken-plate' models of trench-related lithospheric flexure (e.g. Watts & Talwani 1974; Turcotte & Schubert 1982; Solomon & Head 1990). Because our goal is simply the generation of synthetic data, rather than a quantitative analysis of specific bathymetric profiles, the bending moment specified at the trench axis is not a critical factor, regardless. The seaward boundary conditions are represented by the requirement that displacement and plate curvature decay to zero, and we assume that vertical loading occurs only at the trench axis (i.e. at the end of the plate), so that $\sigma_{zz}(x^+, 0) = 0$.

We generate four sets of synthetic inelastic flexural profiles, three of them represent oceanic subduction zones, and the fourth represents proposed lithospheric underthrusting on Venus (e.g. Solomon & Head 1990). Within each set, a single input parameter (either thermal structure or trench depth) is systematically varied to facilitate the recognition of trends in the reliability of Method I flexural analysis. Both thermal structure and trench depth directly influence the degree of lithospheric yielding, and it is anticipated that errors associated with Method-I-type analyses will be greater for higher degrees of lithospheric failure. We also generate several profiles that incorporate significant levels of in-plane force, which will be discussed separately below.

Trench depths are specified with respect to the abyssal plain (not sea-level), or, equivalently, the sea-floor depth at the first zero-crossing. For oceanic flexural profiles, we consider trench depths up to 5 km, which includes the deepest trenches on Earth (e.g. Jarrard 1986), and lithospheric ages of 50 to 150 Ma, which includes most of the commonly analysed trench profiles of the western Pacific. We do not consider variation in sea-floor age along profiles. Because the assumption of uniform sea-floor age implies a constant mechanical plate thickness, it presumably increases the probability that this thickness will be succesfully recovered by our analysis. All flexural profiles relevant to Venus are assigned a 1 km 'trench' depth (e.g. Solomon & Head 1990). Because the primary heat-loss mechanism of Venus remains controversial, we simply assume a range of linear thermal gradients, from 10 to 25 $\mathrm{K\,km}^{-1}$, inclusive, and a surface temperature of 740 K. A 30 $\mathrm{K\,km}^{-1}$ thermal gradient was attempted, but the development of a plastic hinge prevented a unique solution.

For a constant trench depth of 5 km, oceanic flexural profiles are generated for sea-floor ages of 50 to 150 Ma (in 10 Ma intervals), and referred to as Series I (Fig. 5a). Series II and III consist of variable trench depths (1 to 5 km) for constant sea-floor ages of 100 and 50 Ma, respectively (Figs 5b and 5c). Series IV is representative of the flexure of Venusian lithosphere (Fig. 5d).

We also consider oceanic lithosphere that is subjected to significant levels of in-plane force. Although the ridge-push force induced by the elevation of oceanic spreading centres represents a compressional in-plane force, its effects on the

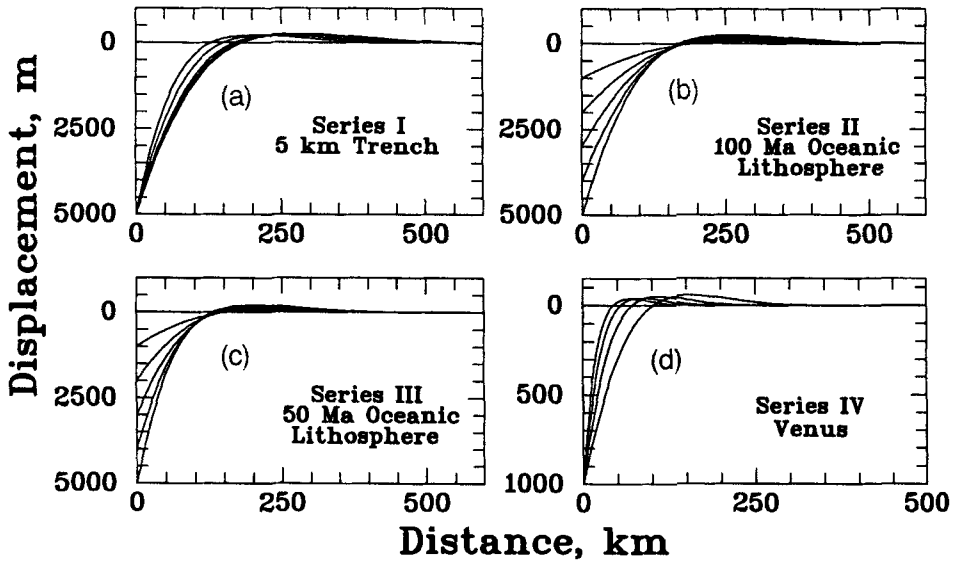

Figure 5. Selected examples of synthetic flexural profiles generated for this study. (a) Series I profiles assume a constant trench depth of 5 km and sea-floor age is incrementally varied from 50 to 150 Ma. Profiles depicted represent sea-floor ages of 50, 70, 100, 120 and 150 Ma (older lithosphere is identifiable by progressively higher outer-rise crests and greater distances to the first zero-crossing). (b) Series II profiles assume a constant sea-floor age of 100 Ma and trench depth is varied incrementally. (c) Series III profiles assume a constant sea-floor age of 50 Ma and trench depth is varied incrementally. (d) Series IV profiles, which represent the flexure of Venusian lithosphere, assume a constant 'trench' depth of 1 km and thermal gradients are varied from 10 to 25 K km^{-1} (lower thermal gradients are identifiable by progressively higher 'outer-rise' crests and greater distances to the first zero-crossing).

flexure of oceanic lithosphere are negligible. This is evident in Fig. 6, which illustrates the moment–curvature relationship for 100 Ma sea-floor subjected to a ridge-push force of -3.5×10^{12} N m^{-1} applied prior to outer-rise plate bending. [This is the maximum ridge-push force predicted on the basis of the cooling-plate model of lithospheric thermal evolution (Parsons & Richter 1980).] For comparison, the moment–curvature relationship for the case of zero in-plane force is also included. The minimal differences between the two moment–curvature relationships indicates that the ridge-push force is unlikely to significantly influence the flexural response of oceanic lithosphere. (Note that this is not necessarily the case for Venusian lithosphere, which may be weaker than oceanic lithosphere.)

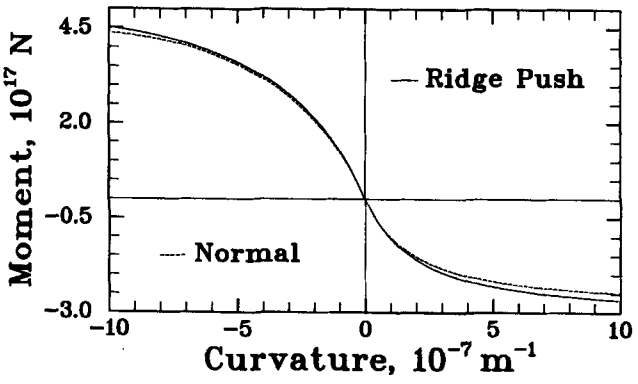

Figure 6. The effects of a nominal ridge-push force on the moment–curvature relationship for 100 Ma oceanic lithosphere (solid line). The assumed value of the compressional in-plane force is -3×10^{12} N m^{-1}, which is the maximum predicted with the cooling-plate model of sea-floor thermal evolution. The broken line represents the moment–curvature relationship for identical lithosphere that is subjected to zero in-plane force; note the relatively small difference between the two curves.

We incoporate much greater levels of in-plane force that are potentially associated with the dynamics of mature subduction zones. Compressional in-plane force an order of magnitude greater than the ridge-push force may result from trench congestion (e.g. Cloetingh & Wortel 1986; McAdoo & Sandwell 1985; Zuber 1987; Mueller & Phillips 1991). Significant levels of tensional in-plane force may also exist if some fraction of the slab-pull force is transmitted into unsubducted portions of the plate (e.g. Spence 1987). The level of in-plane force incorporated into each synthetic profile is constant, which presumably optimizes the likelihood that this value may be accurately recovered. Also, because the assumption of constant in-plane force is routinely adopted in Method-I-type analyses, this assumption strictly simulates the conditions under which such analyses are commonly performed (e.g. Hanks 1971; Watts & Talwani 1974; McAdoo *et al.* 1978; Bodine *et al.* 1981).

We generate flexural profiles consistent with 100 Ma oceanic lithosphere, a 5 km trench depth, and the following levels of in-plane force: (1) a -3×10^{13} N m^{-1} compressional in-plane force applied prior to plate bending (e.g. Fig. 4a), (2) a -3×10^{13} N m^{-1} compressional in-plane force applied subsequent to plate bending (e.g. Fig. 4b); and (3) a $+1.5 \times 10^{13}$ N m^{-1} tensional in-plane force applied prior to plate bending. These values of in-plane force are chosen because they slightly exceed one-half the net lithospheric strength of 100 Ma sea-floor.

As discussed above, in-plane force applied prior to plate bending represents a situation in which this force is initially encountered seawards of the outer-rise complex. In contrast, in-plane force applied subsequent to plate bending implies an initial flexural stress profile (with zero in-plane force) that is abruptly subjected to in-plane compression or tension. For

in-plane compression, this might be the case shortly after a trench becomes congested. Continued, unimpeded convergence along adjacent portions of the trench effectively compresses the oceanic lithosphere seawards of the zone of congestion (Christensen & Ruff 1988; Mueller & Phillips 1991).

The three synthetic flexural profiles that incoporate in-plane force are illustrated in Fig. 7, along with a similar (100 Ma, 5 km trench, etc.) profile with zero in-plane force (broken line). A comparison of the two profiles that incorporate in-plane compression illustrates the influence of loading order on the shape of the outer-rise complex.

6 ELASTIC SOLUTIONS AND FITTING PROCEDURE

During the 'recovery phase' of our analysis, it is assumed that only the shape of the synthetic profile is known. The synthetic profiles are treated as if they were bathymetric (or, in the case of Venusian profiles, altimetric) data. Our objective is to determine if modelling these 'observations' using analytical descriptions of elastic-plate flexure allows the recovery of lithospheric mechanical thickness and/or the level of in-plane force assumed during the generation of the synthetic profiles. This requires a determination of the analytical solution to elastic-plate flexure that most closely resembles each synthetic profile. Elastic-model parameters that are varied during the fitting procedure are the elastic-plate thickness, T_e, the in-plane force, N_e, and the displacement at the trench, w_0. T_e and N_e are varied in increments of 100 m and 2.5×10^{12} N m^{-1}, respectively, and for each combination, w_0 is varied until a minimum misfit is obtained. The latter is varied in increments of 100 m when fitting synthetic flexural profiles that represent oceanic lithosphere, and 10 m when fitting profiles that represent Venusian lithosphere (i.e. Series IV). The best-fitting

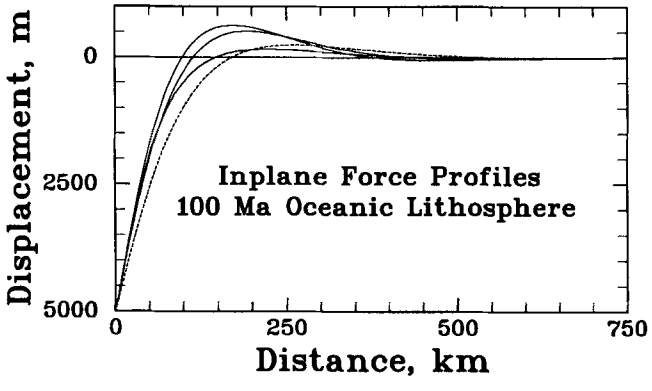

Figure 7. Synthetic profiles that represent the flexure of 100 Ma oceanic lithosphere subjected to significant levels of in-plane force. The highest outer-rise crest corresponds to the synthetic profile that incorporates -3×10^{13} N m^{-1} of in-plane compression applied subsequent to plate bending and the second highest outer-rise crest corresponds to the synthetic profile that incorporates -3×10^{13} N m^{-1} of in-plane compression applied prior to plate bending. The different outer-rise shapes represented in these two profiles illustrates the significance of loading order on lithospheric flexural response. The lowest outer-rise crest corresponds to the synthetic profile that incorporates $+1.5 \times 10^{13}$ N m^{-1} of in-plane tension applied prior to plate bending. The broken line illustrates the synthetic flexure profile that corresponds to identical sea-floor age and trench boundary conditions, but zero in-plane force.

elastic profile does not necessarily exhibit precisely the same trench displacement as the modelled synthetic profile. Unless the elastic solutions indicate plate buckling, however, both displacements are approximately equal.

A trench displacement boundary condition alone is insufficient to specify an elastic solution. We also require that the first zero-crossing of the elastic profile coincide with that of the synthetic profile (this requirement replaces the bending-moment boundary condition at the trench axis). Such a condition not only defines a complete analytical elastic solution (when combined with the requirement that the solution decay to zero seawards of the outer-rise complex), but also reduces the number of candidate elastic profiles to be examined. Preliminary investigations, which incorporated a variety of boundary conditions at the trench axis, confirmed that this constraint does not preclude the best-fitting elastic-plate solutions.

With the trench axis located at $x = 0$ and a plate displacement of w_0, the analytical expression, describing the flexure of an elastic plate subjected to a constant level of in-plane force (N_e), with a first zero-crossing located at x_{zc} is (on the interval $x > 0$)

$$w(x) = A \exp[-\beta(x - x_{zc})] \sin[\alpha(x - x_{zc})], \tag{15}$$

where

$$\beta = \sqrt{\sqrt{\frac{\Delta\rho g}{4D}} + \frac{N_e}{4D}}, \tag{16}$$

$$\alpha = \sqrt{\sqrt{\frac{\Delta\rho g}{4D}} - \frac{N_e}{4D}}, \tag{17}$$

$$A = \frac{w_0}{\exp(\beta x_{zc}) \sin(-\alpha x_{zc})}. \tag{18}$$

The flexural rigidity, D, is defined by the right-hand side of eq. (14), with T_m replaced by T_e.

Misfit is represented by rms residuals of the elastic flexural profiles with respect to the synthetic profiles. Individual residuals are 'sampled' at 1 km intervals out to a distance of 500 km from the trench axis, typically where the seaward end of the outer-rise complex begins to merge with the abyssal plain. Because the specification of the location of the first-crossing implies a bending moment of the trench axis, buckling instabilities are sometimes evident in elastic solutions that assume small values of T_e. This primarily occurs when thin elastic plates are fit to synthetic flexural profiles that exhibit large values of x_{zc}.

7 RESULTS

7.1 Recovery of in-plane force

Fig. 8 illustrates misfit contours, as a function of T_e and N_e, which quantify the degree of dissimilarity between synthetic flexural profiles that incorporate in-plane force and the associated best-fitting elastic solutions. The flat 'central valley' in Fig. 8(a) indicates that, in the case of in-plane compression applied subsequent to plate bending, Method I flexural analysis is insensitive to the assumed value of N_e. In the case of in-plane compression applied prior to plate bending (Fig. 8b), elastic solution misfits exhibit a similar pattern, except that a slight preference is indicated for tensional values of N_e. The important

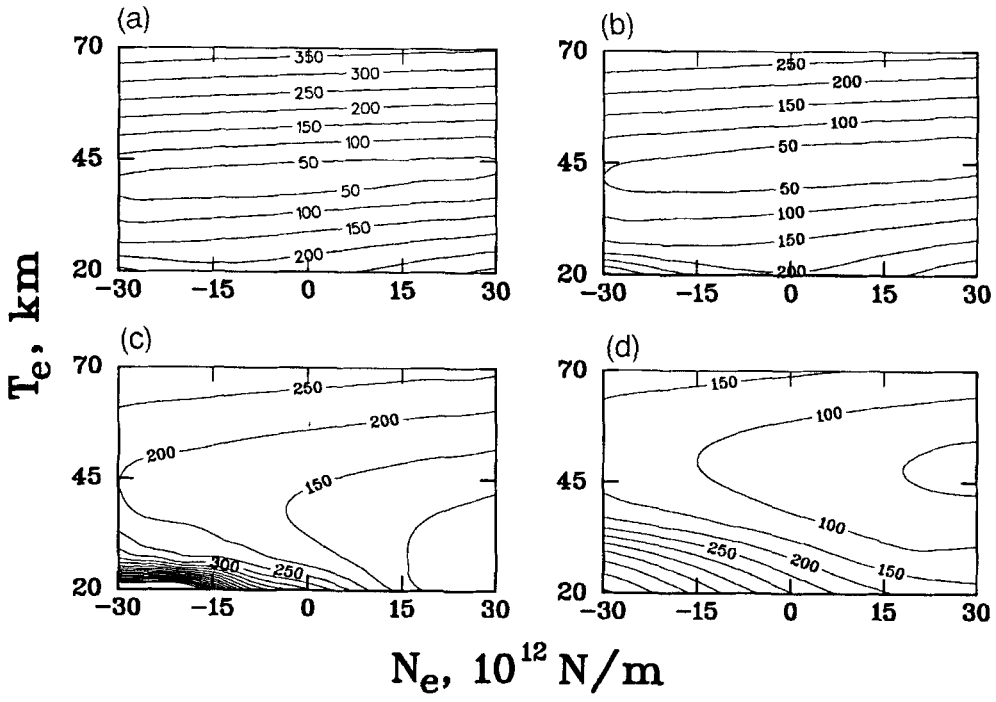

Figure 8. Misfit contours (m), as a function of T_e and N_e, for 100 Ma oceanic lithosphere subjected to significant levels of in-plane force. (a) In-plane compression (-3×10^{13} N m^{-1}) applied subsequent to plate bending. (b) In-plane compression (-3×10^{13} N m^{-1}) applied prior to plate bending. (c) In-plane tension ($+1.5 \times 10^{13}$ N m^{-1}) applied prior to plate bending. Misfit contours indicate that values of in-plane force, N_e, are heavily biased towards excessively tensional values. The extreme levels of misfit in the lower left-hand corner of the diagram are a consequence of the development of buckling instabilities in the elastic-plate solutions. (d) In the case of zero in-plane force, misfit minimization indicates values of in-plane force that are also heavily biased toward excessive tension.

point is that neither Fig. 8(a) nor 8(b) provides a clear indication that the most appropriate value of N_e is -3×10^{13} N m^{-1}. For the remaining synthetic profiles, which incorporate a large tensional in-plane force (Fig. 8c) and zero in-plane force (Fig. 8d), the best-fitting elastic solutions imply values of N_e that exceed the tensional strength of the lithosphere. This bias exists because: (1) the height–width ratio of the outer-rise complex is generally smaller for synthetic profiles than for elastic profiles subjected to the same boundary conditions (including in-plane force), and (2) an increase in N_e decreases the outer-rise amplitude (eq. 16) and increases the outer-rise width (eq. 17) of elastic-plate models. For these reasons, Method I flexural analysis is unlikely to provide reliable estimates of lithospheric in-plane force.

7.2 Recovery of lithospheric mechanical thickness

Elastic-plate thicknesses associated with the best-fitting elastic profiles for Series I–IV synthetic profiles are presented in Tables 2–5; also included are the values of lithospheric mechanical thickness assumed during the generation of each synthetic profile. As expected (e.g. McNutt & Menard 1982; McNutt 1984), T_e is always less than T_m. Also, the results for Series II and III profiles unequivocally indicate that T_e should not be assumed to correspond to any mantle isotherm—a result that is consistent with theoretical arguments presented by McNutt & Menard (1982). These profiles possess variation in trench depth only (i.e. the lithospheric mechanical thickness is constant), yet variation in estimates of T_e exceeds 35 per cent.

We now attempt to recover the lithospheric mechanical thickness assumed during the generation of the synthetic profiles using a method proposed by McNutt & Menard (1982). This method establishes a correspondence between T_e and T_m that is based upon the requirement that, for a specified curvature, the lithospheric plate and the representative elastic plate support identical bending moments (Fig. 9). The most appropriate plate curvature upon which to base such a correspondence principle is not immediately obvious. Although McNutt (1984) has proposed, on the basis of theoretical considerations, that the most reliable conversions should be based on the maximum curvature of the subducting lithosphere (as indicated by the bathymetric profile), in practice the first zero-crossing curvature of the best-fitting elastic profiles has been substituted as a more practical alternative (e.g. McNutt & Menard 1982; McNutt 1984; Solomon & Head 1990; Sandwell & Schubert 1992). Although it is reasonable to assume that there exists some value of plate curvature at which the conversion procedure will result in the exact recovery of the T_m, whether such a curvature coincides with either of the above alternatives, or, in fact, even remains invariant with respect to different flexural profiles, has not been determined.

Simple intuitive considerations provide some insight regarding the choice of an appropriate conversion curvature. For a specified plate curvature, the bending moment of an inelastic plate decreases with decreasing mechanical thickness and/or increasing degrees of failure. Because the extent of failure is strongly correlated with plate curvature, a conversion curvature that is 'too small' would imply an unrepresentatively small degree of failure. The conversion procedure would compensate for this with a reduction in the mechanical thickness of the lithospheric plate. In other words, if the adopted conversion curvature is 'too small', the lithospheric mechanical thickness

Table 2. Series I mechanical thickness errors (defined as the difference between the assumed and recovered values of T_m divided by the assumed value). T_m and T_e represent the assumed lithospheric mechanical thickness and the elastic-plate thickness associated with the best-fitting elastic profile, respectively. The next four columns indicate errors corresponding to the conversion procedure based upon the following variations of conversion curvatures: (1) the first zero-crossing curvature of the synthetic profile (Fig. 10a); (2) the first zero-crossing curvature of the best-fitting elastic profile (Fig. 10b); (3) the maximum curvature of the synthetic profile (Fig 10c), and (4) the maximum curvature of the best-fitting elastic profile (Fig. 10d). A negative mechanical thickness error indicates that the recovered value is excessive. The final column specifies the ratio of the maximum bending moment supported in the synthetic profile to the saturation moment that is characteristic of the relevant yield envelope (a convenient measure of the degree of bending-induced inelasticity).

Series I	$T_m(km)$	$T_e(km)$	V1 Error	V2 Error	V3 Error	V4 Error	$\frac{M_{max}}{M_{sat}}$
50 Ma	48.08	33.15	+0.152	+0.105	-0.152	+0.015	0.816
60 Ma	52.40	37.50	+0.131	+0.091	-0.128	+0.004	0.784
70 Ma	56.07	40.60	+0.130	+0.097	-0.093	+0.015	0.758
80 Ma	59.10	43.80	+0.116	+0.088	-0.085	+0.010	0.736
90 Ma	61.57	46.40	+0.106	+0.079	-0.077	-0.003	0.718
100 Ma	63.53	48.30	+0.103	+0.079	-0.070	-0.005	0.702
110 Ma	65.09	49.75	+0.101	+0.079	-0.060	+0.008	0.690
120 Ma	66.32	50.95	+0.100	+0.079	-0.055	-0.009	0.679
130 Ma	67.29	51.90	+0.098	+0.079	-0.051	+0.010	0.671
140 Ma	68.05	52.60	+0.098	+0.079	-0.047	+0.012	0.665
150 Ma	68.64	53.20	+0.097	+0.079	-0.046	+0.012	0.660

Table 3. Series II mechanical thickness errors (see Table 2 caption).

Series II	$T_m(km)$	$T_e(km)$	V1 Error	V2 Error	V3 Error	V4 Error	$\frac{M_{max}}{M_{sat}}$
1 km	63.53	61.20	+0.013	+0.012	-0.012	-0.010	0.203
2 km	63.53	57.80	+0.031	+0.024	-0.029	-0.019	0.369
3 km	63.53	53.85	+0.061	+0.052	-0.028	-0.003	0.504
4 km	63.53	50.70	+0.085	+0.070	-0.037	+0.005	0.615
5 km	63.53	48.30	+0.103	+0.079	-0.070	-0.005	0.702

Table 4. Series III mechanical thickness errors (see Table 2 caption).

Series III	$T_m(km)$	$T_e(km)$	V1 Error	V2 Error	V3 Error	V4 Error	$\frac{M_{max}}{M_{sat}}$
1 km	48.08	45.40	+0.019	+0.017	-0.021	-0.015	0.275
2 km	48.08	40.60	+0.075	+0.068	-0.015	+0.015	0.480
3 km	48.08	37.35	+0.108	+0.090	-0.036	+0.023	0.631
4 km	48.08	35.25	+0.125	+0.093	-0.091	+0.012	0.739
5 km	48.08	33.15	+0.152	+0.105	-0.152	+0.015	0.816

Table 5. Series IV mechanical thickness errors (see Table 2 caption).

Series IV	$T_m(km)$	$T_e(km)$	V1 Error	V2 Error	V3 Error	V4 Error	$\frac{M_{max}}{M_{sat}}$
10 K/km	31.32	26.90	+0.068	+0.057	-0.041	-0.003	0.537
15 K/km	20.88	16.70	+0.107	+0.078	-0.094	-0.003	0.705
20 K/km	15.66	11.40	+0.152	+0.101	-0.175	+0.006	0.814
25 K/km	12.53	8.35	+0.185	+0.106	-0.316	-0.000	0.892

is likely to be underestimated. Conversely, if the adopted conversion curvature is 'too large', the lithospheric mechanical thickness is likely to be overestimated. In this case, the amount of failure implied by the assumed plate curvature will be excessive, and a greater mechanical thickness is necessary to achieve the specified moment–curvature ratio (i.e. the implied excessive failure would tend to reduce this ratio and a greater value of T_m would be necessary to compensate for this).

Conversions are performed in the following manner. For a specified plate curvature, the corresponding bending moment is calculated for a series of yield envelopes (representing various values of T_m), and in each case the thickness of the elastic

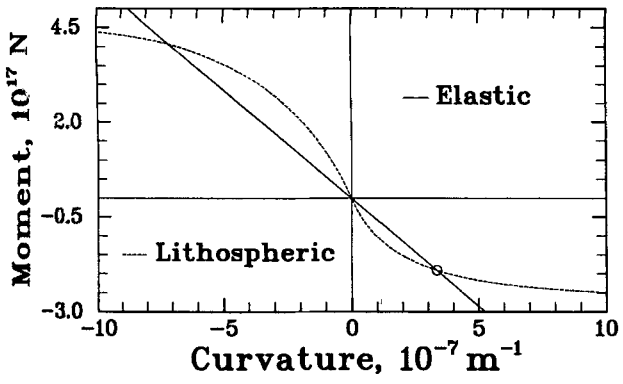

Figure 9. The correspondence between elastic-plate thickness and lithospheric mechanical thickness is based upon the requirement that both plates support identical bending moments at a specified curvature (denoted by the circle).

plate that supports an identical bending moment at the same plate curvature is also determined. This establishes a relationship beween T_e and T_m, which is based on the assumed value of plate curvature (e.g. McNutt 1984). We perform this procedure using the following conversion curvatures: (1) the *first zero-crossing* curvature of the *synthetic* profile; (2) the *first-zero-crossing* curvature of the *best-fitting elastic* profile, (3) the *maximum* curvature of the *synthetic* profile; and (4) the *maximum* curvature of the *best-fitting elastic* profile.

Mechanical thickness errors (defined as the difference between the original and recovered values of T_m divided by the original value) are presented in Tables 2–5. Negative errors indicate that the lithospheric mechanical thickness has been overestimated. In Fig. 10 these errors are displayed as a function of the ratio of maximum bending moment represented in the synthetic flexural profile and the saturation bending moment associated with the assumed lithospheric yield envelope. This ratio represents a convenient measure of the degree of lithospheric failure (i.e. inelasticity) associated with plate bending. Results are presented in this manner because it is anticipated that errors associated with Method I flexural analysis will correlate with the degree of inelastic behaviour represented in the synthetic flexural profile. Such a trend is, in fact, clearly evident in Figs 10(a) and (b). These figures also indicate a consistent underestimation of the lithospheric mechanical thickness, suggesting that the first zero-crossing curvatures of both flexural profiles are too small.

Fig. 10(c) indicates that Variation 3 conversions (based on maximum synthetic plate curvature) produce significantly improved estimates of T_m, provided that the maximum bending moment in the synthetic profile does not exceed 65 per cent of the corresponding moment saturation value. Beyond this point, Variation 3 progressively overestimates lithospheric mechanical thickness. This occurs because, as the amount of bending-induced failure increases, the maximum plate curvature becomes progressively localized and eventually begins to exhibit a pronounced difference from neighbouring values. In extreme cases, this culminates in the development of a plastic hinge, and the maximum plate curvature may become arbitrarily large. It is therefore not surprising that the maximum synthetic plate curvature may significantly overestimate the amount of failure in neighbouring regions of the plate, and the conversion procedure that we have labelled Variation 3 will overestimate lithospheric mechanical thickness.

Fig 10(d) illustrates that Variation 4, the conversion based on the maximum curvature of the best-fitting elastic profile, is the most reliable variation considered. The difficulties associated with Variation 3 are avoided because the localization of maximum curvature is a phenomenon uniquely characteristic of inelastic-plate bending. The error associated with Variation 4 rarely exceeds 2 per cent, and lithospheric mechanical thickness is neither consistently overestimated nor consistently

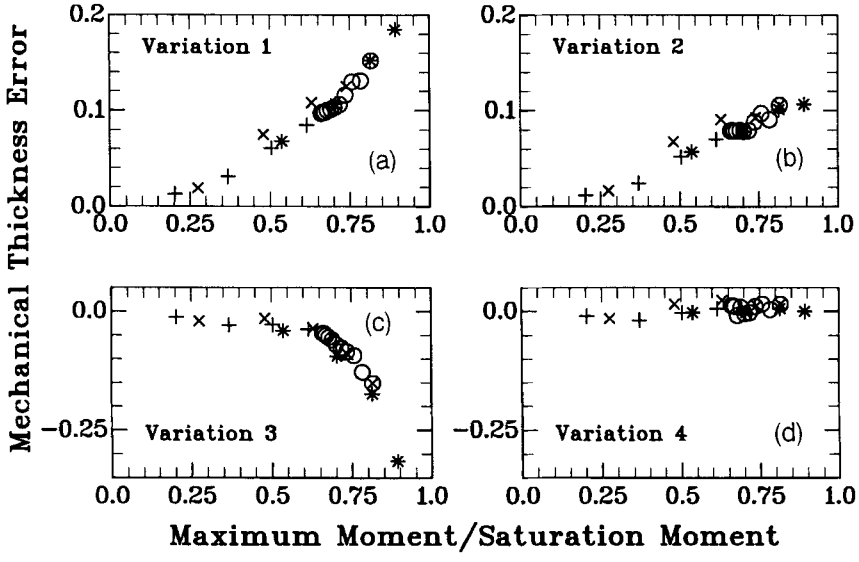

Figure 10. Mechanical thickness error (difference between the original and recovered values of T_m, divided by the original value) plotted with respect to the ratio of maximum bending moment and the saturation moment (a convenient measure of the degree of inelastic behaviour). (a) Conversion using the first zero-crossing curvature of the synthetic profile (Variation 1). (b) Conversion using the first zero-crossing curvature of the best-fitting elastic profile (Variation 2). (c) Conversion using the maximum curvature of the synthetic profile (Variation 3). (d) Conversion using the maximum curvature of the best-fitting elastic profile (Variation 4). Symbols denote Series I (○), Series II (+), Series III (×), and Series IV (*) profiles.

underestimated. The relationship between the mechanical thickness error and the degree of bending-induced failure exhibits no indication of an increasing trend to at least 90 per cent of the bending-moment saturation value.

For each of the four variations of the conversion procedure, the results for the Venusian profiles share the trends exhibited by the oceanic profiles. This suggests that the principles governing the relationship between mechanical thickness error and the manner in which T_e is converted into T_m are robust and therefore relevant to a wide range of flexural problems.

Assuming that accurate estimates of T_e are possible, a slight modification of the conversion procedure proposed by McNutt & Menard (1982) produces surprisingly reliable estimates of lithospheric mechanical thickness. In practice, however, there may be serious difficulties in determining T_e due to complications associated with bathymetric (or altimetric) noise. This is illustrated in Fig. 11. In Fig. 11(a), misfit values are displayed, as a function of T_e, for the synthetic profile representing 100 Ma oceanic lithosphere subjected to zero in-plane force and a 5 km trench displacement [essentially a 'slice' through Fig. 8(d) at $N_e = 0$]. The corresponding best-fitting elastic profile ($T_e = 48.3$ km) is shown in Fig. 11(b) (solid line), along with the synthetic profile (broken line). The broad curvature exhibited in Fig. 11(a), particularly in the neighbourhood of the minimum rms misfit, indicates that relatively small differences in misfit correspond to large differences in estimates of T_e.

Bathymetric (as well as altimetric) profiles typically reveal ubiquitous topographic irregularities that are approximately 50–100 m in amplitude (Caldwell *et al.* 1976; Turcotte *et al.* 1978; Bodine *et al.* 1981; McQueen & Lambeck 1989; Solomon & Head 1990). For the example presented in Fig. 11(a) a 50 m standard deviation in data would correspond to $34.3 \text{ km} \leq T_e \leq 64.1$ km. In other words, in the presence of significant bathymetric noise, T_e might be associated with errors as large as 15 km. The best-fitting elastic profiles that correspond to these bounding values of elastic-plate thickness are shown in Figs 11(c) and (d).

There is an additional difficulty. Fig. 8 illustrates that in-plane force can significantly influence estimates of T_e and, consequently, interpretations of lithospheric mechanical thickness. This is most evident in the 'valley' that cuts across Fig. 8(c) in a strongly diagonal fashion. Although the other cases represented in Fig. 8 do not exhibit as pronounced a dependence between estimates of T_e and assumed values of N_e, variations in T_e of up to 5 km are indicated within the limits of N_e considered. Fig. 8 (particularly Fig. 8c) represents a warning that uncertainties associated with in-plane force may undermine the reliability of lithospheric constraints determined with Method I flexural analysis, even in the absence of topographic noise.

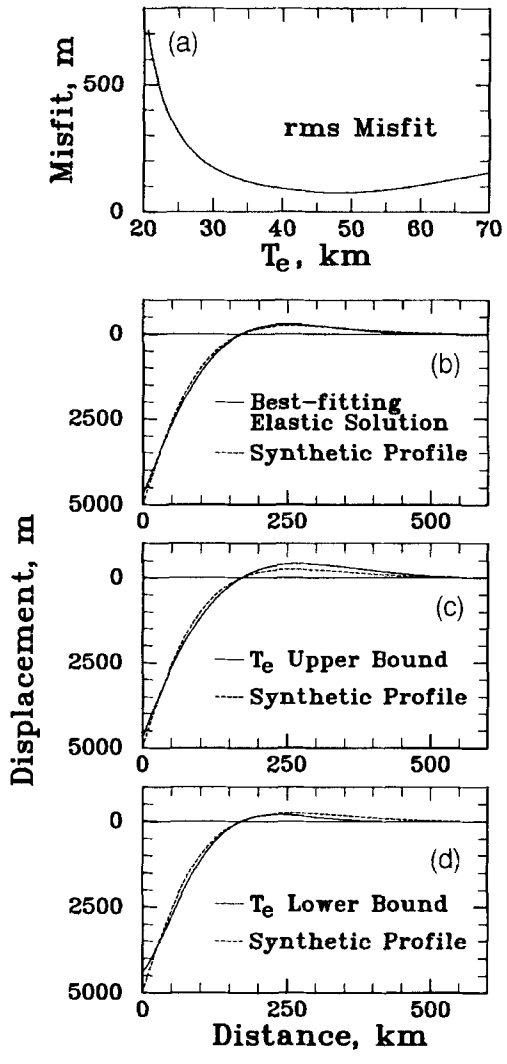

Figure 11. (a) Minimum misfit, plotted with respect to T_e, between an elastic model assuming $N_e = 0$ (a 'slice' through Fig. 8d at $N_e = 0$) and a synthetic profile representing 100 Ma oceanic lithosphere subjected to zero in-plane force and a 5 km trench displacement. The relative flatness of the curve indicates that small differences in misfit, such as those that might result from bathymetric noise, may result in significant errors in estimates of T_e. (b) Best-fitting elastic solution corresponding to (a), $T_e = 48.3$ km. (c) Best-fitting elastic solution corresponding to the upper bound on T_e (64.1 km; see text). (d) Best-fitting elastic solution corresponding to the lower bound on T_e (34.3 km; see text).

8 CONCLUSIONS

We have examined the common practice of constraining lithospheric mechanical thickness and in-plane force using elastic models of outer-rise flexure. This was accomplished by: (1) numerically generating flexural profiles consistent with both empirically derived constraints on lithospheric rheology and trench-type boundary conditions; (2) determining the elastic-plate flexural profiles that most closely approximate the shape of these 'synthetic' profiles; and (3) attempting to recover lithospheric parameters incoporated into the synthetic profiles from the best-fitting elastic solutions.

It was unequivocally determined that elastic models of plate flexure cannot provide reliable constraints on in-plane force (i.e. regional stress). It is not even possible to distinguish the qualitative nature of in-plane force (i.e. compressional versus tensional).

Attempts to constrain the lithospheric mechanical thickness using elastic models of plate flexure require that the best-fitting elastic plate thickness, T_e, be interpreted in terms of the lithospheric mechanical structure. Several early flexural studies pursued the possibility that T_e simply corresponded to the depth of a particular mantle isotherm (e.g. Watts 1978; Caldwell & Turcotte 1979). McNutt & Menard (1982) concluded that

such an interpretation of T_e was too simplistic, and that any correspondence between T_e and lithospheric mechanical structure must be influenced by plate curvature. Our results are consistent with this conclusion.

We evaluated the reliability of a method proposed by McNutt & Menard (1982) to convert values of T_e into estimates of lithospheric mechanical thickness, T_m. The conversion procedure utilized is based upon the requirement that both elastic and inelastic (i.e. lithospheric) plates maintain identical bending moments at a specified value of plate curvature. Previous investigations have used the first zero-crossing curvature of the best-fitting elastic solution (McNutt & Menard 1982; McNutt 1984; Solomon & Head 1990), which our results indicate may be associated with errors in T_m of up to 10 per cent. Although such an error is not serious for many applications of lithospheric flexural analysis, it can be significant when attempting to identify trends in thermal evolution. We have determined that the optimal conversion curvature is the maximum curvature of the best-fitting elastic profile (<2 per cent error). This conclusion is inconsistent with theoretical arguments (McNutt 1984), suggesting that the optimal curvature is the maximum curvature of the lithospheric (or synthetic) plate. The reliability of the latter variation of the conversion procedure is comparable to that which uses the maximum curvature of the best-fitting elastic profile only when the maximum bending moment sustained by the subducting plate does not exceed 65 per cent of the saturation value. Beyond this point, the maximum curvature of the subducting plate becomes progressively localized and unrepresentative of regional flexure.

Although, in principle, elastic-plate models of outer-rise flexure offer reliable constraints on the mechanical thickness of the lithosphere, in practice uncertainties associated with bathymetric noise and in-plane force may, in some cases, preclude rigorous conclusions. Estimates of T_m based on elastic-plate models of lithospheric flexure are, at best, as reliable as the associated estimates of T_e. Faulty assumptions regarding the level of ambient in-plane force may introduce uncertainties in determinations of T_e that range from 5 to 20 km (i.e. $\simeq$10 to 40 per cent), with the greatest uncertainty resulting from the inability to recognize the existence of significant levels of in-plane tension. Bathymetric noise may also introduce a comparable degree of uncertainty.

ACKNOWLEDGMENTS

We acknowledge useful conversations with David Blackwell, Ian Duncan, Bob Grimm, Vicki Hansen and Paul Morgan, as well as constructive reviews from David Sandwell and Maria Zuber. This work was supported by NASA Grant NAGW-3024 from the Planetary Geology and Geophysics Program at Washington University.

REFERENCES

Bodine, J.H. & Watts, A.B., 1979. On lithospheric flexure seaward of the Bonin and Mariana Trenches, *Earth planet. Sci. Lett.*, **43,** 132–148.

Bodine, J.H., Steckler, M.S. & Watts, A.B., 1981. Observations of flexure and rheology of the oceanic lithosphere, *J. geophys. Res.*, **86,** 3695–3707.

Brace, W.F. & Kohlstedt, D.L., 1980. Limits on lithospheric stress imposed by laboratory experiments, *J. geophys. Res.*, **85,** 6248–6252.

Byerlee, J., 1978. Friction of rocks, *Pure appl. Geophys.*, **116,** 615–626.

Caldwell, J.G. & Turcotte, D.L., 1979. Dependence of the thickness of the elastic oceanic lithosphere on age, *J. geophys. Res.*, **84,** 7572–7576.

Caldwell, J.G., Haxby, W.F., Karig, D.E. & Turcotte, D.L., 1976. On the applicability of a universal elastic trench profile, *Earth planet. Sci. Lett.*, **31,** 239–246.

Chapple, W.M. & Tullis, T.E., 1977. Evaluation of the forces that drive the plates, *J. geophys. Res.*, **82,** 1967–1984.

Christensen, D.H. & Ruff, L.J., 1988. Seismic coupling and outer rise earthquakes, *J. geophys. Res.*, **93,** 13 421–13 444.

Cloetingh, S. & Wortel, R. 1986. Stress in the Indo-Australian plate, *Tectonophysics*, **132,** 49–67.

Craig, C.H. & McKenzie, D., 1986. The existence of a thin low-viscosity layer beneath the lithosphere, *Earth planet. Sci. Lett.*, **78,** 420–426.

Drucker, D.C., 1967. *Introduction to Mechanics of Deformable Solids*, McGraw-Hill, New York, NY.

Forsyth, D. & Uyeda, S., 1975. On the relative importance of the driving forces of plate motion, *Geophys. J.*, **43,** 163–200.

Fung, Y.C., 1965. *Foundations of Solid Mechanics*, Prentice-Hall, Englewood Cliffs, NJ.

Goetze, C. & Evans, B., 1979. Stress and temperature in the bending of lithosphere as constrained by experimental rock mechanics, *Geophys. J.*, **59,** 463–478.

Hanks, T.C., 1971. The Kuril Trench–Hokkaido Rise system: Large shallow earthquakes and simple models of deformation, *Geophys. J.*, **23,** 173–189.

Hyndman, R.D., Langseth, M.G. & von Herzen, R.P., 1987. Deep sea drilling project geothermal measurements: A review, *Rev. Geophys.*, **25,** 1563–1582.

Jaeger, J.C. & Cook, N.G.W., 1976. *Fundamentals of Rock Mechanics*, John Wiley, New York, NY.

Janle, P., Jannsen, D. & Basilevsky, A.T., 1988. Tepev Mons on Venus: Morphology and elastic bending models, *Earth Moon Planets*, **41,** 127–139.

Jarrard, R.D., 1986. Relations among subduction parameters, *Rev. Geophys.*, **24,** 217–284.

Johnson, W. & Mellor, P.B., 1973. *Engineering Plasticity*, Van Nostrand Reinhold, London.

Johnson, C.L. & Sandwell, D.T., 1994. Lithospheric flexure on Venus, *Geophys. J. Int.*, **119,** 627–647.

Judge, A. & NcNutt, M., 1988. The relationship between plate curvature and elastic plate thickness: A study of the Peru–Chile Trench (abstract), *EOS, Trans. Am. geophys. Un.* **69,** 468.

Kaula, W.M. & Phillips, R.J., 1981. Quantitative tests for plate tectonics on Venus, *Geophys. Res. Lett.*, **8,** 1187–1190.

Kirby, S.H., 1983. Rheology of the lithosphere, *Rev. Geophys.*, **21,** 1458–1487.

McAdoo, D.C. & Martin, C.F., 1984. Seasat observations of lithospheric flexure seaward of trenches, *J. geophys. Res.*, **89,** 3201–3210.

McAdoo, D.C. & Sandwell, D.T., 1985. Folding of oceanic lithosphere, *J. geophys. Res.*, **90,** 8563–8569.

McAdoo, D.C., Caldwell, J.G. & Turcotte, D.L., 1978. On the elastic–perfectly plastic bending of the lithosphere under generalized loading with application to the Kuril Trench, *Geophys. J.*, **54,** 11–26.

McAdoo, D.C., Martin, C.F. & Poulouse, S., 1985. Seasat observations of flexure: Evidence for a strong lithosphere, *Tectonophysics*, **116,** 209–222.

McNutt, M.K., 1984. Lithospheric flexure and thermal anomalies, *J. geophys. Res.*, **89,** 11 180–11 194.

McNutt, M.K. & Menard, H.W., 1982. Constraints on yield strength in the oceanic lithosphere from observations of flexure, *Geophys. J.*, **71,** 363–394.

McQueen, H.W.S. & Lambeck, K., 1989. The accuracy of some lithospheric banding parameters, *Geophys. J.*, **96,** 401–413.

Melosh, J., 1977. Shear stress on the base of a lithospheric plate, *Pure appl. Geophys.*, **115,** 429–439.

Morgan, P. & Phillips, R.J., 1983. Hot spot heat transfer: Its application of Venus and implications to Venus and Earth, *J. geophys. Res.*, **88**, 8305–8317.

Mueller, S. & Phillips, R.J., 1991. On the initiation of subduction, *J. geophys. Res.*, **96**, 651–665.

Parsons, B. & Molnar, P., 1976. The origin of outer topographic rises associated with trenches, *Geophys. J. R. astr. Soc.*, **45**, 707–712.

Parsons, B. & Richter, F.M., 1980. A relation between the driving force and geoid anomaly associated with mid-ocean ridges, *Earth planet. Sci. Lett.*, **51**, 445–450.

Parsons, B. & Sclater, J.G., 1977. An analysis of the variation of ocean floor bathymetry and heat flow with age, *J. geophys. Res.*, **82**, 803–827.

Phillips, R.J., 1990. Convection-driven tectonics on Venus, *J. geophys. Res.*, **95**, 1301–1316.

Phillips, R.J. & Malin, M.C., 1983. The interior of Venus and tectonic implications, in *Venus*, pp. 159–214, eds Hunten, D.M., Colin, L., Donahue, T.M. & Moroz, V.I., University of Arizona Press, Tucson, AZ.

Sandwell, D.T. & Schubert, G., 1992. Flexural ridges, trenches, and outer rises around coronae on Venus, *J. geophys. Res.*, **97**, 16 069–16 083.

Solomon, S.C. & Head, J.W., 1982. Mechanisms for lithospheric heat transport on Venus: Implications for tectonic style and volcanism, *J. geophys. Res.*, **87**, 9236–9246.

Solomon, S.C. & Head, J.W., 1990. Lithospheric flexure beneath the Freyja Montes Foredeep, Venus: Constraints on lithospheric thermal gradient and heat flow, *Geophys. Res. Lett.*, **17**, 1393–1396.

Spence, W., 1987. Slab pull and seismotectonics of subducting lithosphere, *Rev. Geophys.*, **25**, 55–69.

Turcotte, D.L. & Schubert, G., 1982. *Geodynamics: Applications of Continuum Physics to Geological Problems*, John Wiley, New York, NY.

Turcotte, D.L., McAdoo, D.C. & Caldwell, J.G., 1978. An elastic–perfectly plastic analysis of the bending of the lithosphere at a trench, *Tectonophysics*, **47**, 193–205.

Watts, A.B., 1978. An analysis of isostasy in the World's oceans: 1. Hawaiian-Emperor Seamount Chain, *J. geophys. Res.*, **83**, 5989–6004.

Watts, A.B. & Talwani, M., 1974. Gravity anomalies seaward of deep-sea trenches and their tectonic implications, *Geophys. J.*, **36**, 57–90.

Watts, A.B., Bodine, J.H. & Steckler, M.S., 1980. Observations of flexure and the state of stress in the oceanic lithosphere, *J. geophys. Res.*, **85**, 6369–6376.

Wessel, P., 1992. Thermal stresses and the bimodal distribution of elastic thickness estimates of the oceanic lithosphere, *J. geophys. Res.*, **97**, 14 177–14 193.

Wiens, D.A. & Stein, S., 1985. Implications of oceanic intraplate seismicity for plate stresses, driving forces, and rheology, *Tectonophysics*, **116**, 143–162.

Zuber, M.T., 1987. Compression of oceanic lithosphere: An analysis of intraplate deformation in the Central Indian basin, *J. geophys. Res.*, **92**, 4817–4825.

APPENDIX A: DERIVATION OF EQS (10) AND (11)

Assuming a frictional relationship of the nature

$$\tau = \tau_0 + \mu\bar{\sigma}_n, \tag{A1}$$

where τ is shear resistance, $\bar{\sigma}_n$ is effective normal stress (i.e. normal stress minus pore pressure), and τ_0 and μ are empirically determined constants, Jaeger & Cook (1976) determined that the minimum differential stress required to promote brittle failure is

$$\Delta\sigma = \sigma_1 - \sigma_3 = 2(\tau_0 + \mu\bar{\sigma}_3)(\sqrt{\mu^2+1} + \mu), \tag{A2}$$

where σ_1 and σ_3 are the maximum and minimum principal stresses, respectively, and $\bar{\sigma}_3$ equals σ_3 minus the ambient pore pressure. Eq. (A2) assumes the existence of faults that are oriented in such a manner as to minimize the resistance to frictional sliding. If such faults are unavailable, brittle lithospheric strength will exceed estimates based on (A2). Eq. (A2) may be expressed in the form

$$\Delta\sigma = a\bar{\sigma}_3 + b, \tag{A3}$$

with

$$a = 2\mu(\sqrt{\mu^2+1} + \mu), \tag{A4}$$

and

$$b = 2\tau_0(\sqrt{\mu^2+1} + \mu). \tag{A5}$$

Byerlee (1978) determined that the frictional characteristics of rock are essentially independent of temperature, slip rate, and, in most cases, composition. The empirically determined relationship that quantifies the frictional behaviour of rock is

$$\tau = \begin{cases} 0.85\sigma_n & \sigma_n \le 200\ \text{MPa}, \\ 0.6\sigma_n + 50\ \text{MPa} & \sigma_n \ge 200\ \text{MPa}. \end{cases} \tag{A6}$$

For the low-stress branch of Byerlee's Law, $a = 3.68$ and $b = 0$. For the high-stress branch of Byerlee's Law, $a = 2.12$ and $b = 176.6$.

Compressional brittle strength

In the case of compression, we equate σ_1 with the horizontal tectonic stress σ_{xx}, and σ_3 with the lithospheric overburden σ_{zz}:

$$\begin{aligned} \Delta\sigma = \sigma_{xx} - \sigma_{zz} &= a\bar{\sigma}_3 + b \\ &= a\bar{\sigma}_{zz} + b \\ &= \begin{cases} 3.68\bar{\sigma}_{zz} & \bar{\sigma}_{zz} \le 113.2\ \text{MPa}, \\ 2.12\bar{\sigma}_{zz} + 176.6\ \text{MPa} & \bar{\sigma}_{zz} \ge 113.2\ \text{MPa}. \end{cases} \end{aligned} \tag{A7}$$

Tensional brittle strength

In the case of tension, we equate σ_1 with the lithospheric overburden σ_{zz}, and σ_3 with the horizontal tectonic stress σ_{xx}:

$$\Delta\sigma = \sigma_1 - \sigma_3 = \sigma_{zz} - \sigma_{xx} = a\bar{\sigma}_3 + b = a\bar{\sigma}_{xx} + b.$$

Noting that $\sigma_{zz} - \sigma_{xx} = \bar{\sigma}_{zz} - \bar{\sigma}_{xx}$, and solving for $\bar{\sigma}_{xx}$, we have

$$\bar{\sigma}_{xx} = \frac{\bar{\sigma}_{zz} - b}{1 + a}, \tag{A9}$$

so that

$$\begin{aligned} \Delta\sigma = \bar{\sigma}_{zz} - \bar{\sigma}_{xx} &= \frac{a\bar{\sigma}_{zz} + b}{1 + a} \\ &= \begin{cases} 0.786\bar{\sigma}_{zz} & \bar{\sigma}_{zz} \le 529.9\ \text{MPa}, \\ 0.679\bar{\sigma}_{zz} + 56.7\ \text{MPa} & \bar{\sigma}_{zz} \ge 529.9\ \text{MPa}. \end{cases} \end{aligned} \tag{A10}$$